Naval Research Laboratory
Washington, DC 20375-5000

(2)

NRL Memorandum Report 6372

Acousto-Optical Vector Matrix Product Processor: Implementation Issues

EUGENE P. MOSCA

Department of Physics
United States Naval Academy

FRANK P. PURSEL, RICHARD D. GRIFFIN AND JOHN N. LEE

Applied Optics Branch
Optical Sciences Division

April 25, 1989

SECURITY CLASSIFICATION OF THIS PAGE

REPORT DOCUMENTATION PAGE

Form Approved OMB No. 0704-0188

1a. REPORT SECURITY CLASSIFICATION: UNCLASSIFIED	1b. RESTRICTIVE MARKINGS
2a. SECURITY CLASSIFICATION AUTHORITY	3. DISTRIBUTION/AVAILABILITY OF REPORT: Approved for public release; distribution unlimited.
2b. DECLASSIFICATION/DOWNGRADING SCHEDULE	
4. PERFORMING ORGANIZATION REPORT NUMBER(S): NRL Memorandum Report 6372	5. MONITORING ORGANIZATION REPORT NUMBER(S)
6a. NAME OF PERFORMING ORGANIZATION: Naval Research Laboratory; 6b. OFFICE SYMBOL (If applicable): Code 6530	7a. NAME OF MONITORING ORGANIZATION
6c. ADDRESS (City, State, and ZIP Code): Washington, DC 20375-5000	7b. ADDRESS (City, State, and ZIP Code)
8a. NAME OF FUNDING/SPONSORING ORGANIZATION: Office of Naval Technology; 8b. OFFICE SYMBOL (If applicable)	9. PROCUREMENT INSTRUMENT IDENTIFICATION NUMBER
8c. ADDRESS (City, State, and ZIP Code): Arlington, VA 22217-5000	10. SOURCE OF FUNDING NUMBERS: PROGRAM ELEMENT NO: PE 62314; PROJECT NO: RJ 14C37; TASK NO: ; WORK UNIT ACCESSION NO: DN380-062

11. TITLE (Include Security Classification)
Acousto-Optical Vector Matrix Product Processor: Implementation Issues

12. PERSONAL AUTHOR(S)
Mosca,* E.P., Pursel, F.P. Lt., Griffin, R.D. and Lee, J.N.

13a. TYPE OF REPORT	13b. TIME COVERED	14. DATE OF REPORT (Year, Month, Day)	15. PAGE COUNT
	FROM _____ TO _____	1989 April 25	27

16. SUPPLEMENTARY NOTATION
*Department of Physics United States Naval Academy

17. COSATI CODES			18. SUBJECT TERMS (Continue on reverse if necessary and identify by block number)
FIELD	GROUP	SUB-GROUP	Acousto-optical; Diode laser; Vector matrix product; Optical processing

19. ABSTRACT (Continue on reverse if necessary and identify by block number)

An Acousto-Optic Technique is used to design and construct a prototype of a processor capable of multiplying a 128 x 128 element matrix by a 128 element vector. The elements of the matrix and the vectors are complex numbers. The device is specified to execute 10^5 vector/matrix products per second with 8-bit accuracy. The performance of each component of the prototype was evaluated as was the impact of component performance on system performance.

20. DISTRIBUTION/AVAILABILITY OF ABSTRACT: ☒ UNCLASSIFIED/UNLIMITED ☐ SAME AS RPT ☐ DTIC USERS	21. ABSTRACT SECURITY CLASSIFICATION: UNCLASSIFIED
22a. NAME OF RESPONSIBLE INDIVIDUAL: John N. Lee	22b. TELEPHONE (Include Area Code): (202) 767-3100; 22c. OFFICE SYMBOL: Code 6537

DD Form 1473, JUN 86 — Previous editions are obsolete — SECURITY CLASSIFICATION OF THIS PAGE

S/N 0102-LF-014-6603

CONTENTS

ACOUSTO-OPTICAL VECTOR MATRIX PRODUCT PROCESSOR: IMPLEMENTATION ISSUES

I. INTRODUCTION

An acousto-optic (AO) vector matrix multiplier (VMM) may be conceived of as a high speed pipelined processor. Present AO technology promises to allow multiplication of 128-element vectors by a 128 x 128 element matrix at a rate of 10^5 vector-matrix products per second. The vector components, along with the matrix elements, are complex numbers whose real and imaginary parts are each 8-bit signed numbers. While such a processor may be used for any linear transformation, our immediate interest is in the computation of discrete Fourier transforms.

The rate of 10^5 such vector-matrix products per second requires eight-bit integer products at a rate of approximately 1.7×10^{12} multiplies per second. This rate is not achievable with current digital technology. A prototype processor (rack mountable 19" chassis not to exceed 9 inches in height) using AO technology was designed and assembled by Westinghouse R&D Center and evaluated by the Applied Optics Branch of the Naval Research Laboratory. This report consists of a descriptive system overview, a component by component performance evaluation, a system performance evaluation, and suggestions for future development in this area.

II. SYSTEM OVERVIEW

A schematic diagram of the VMM processor is illustrated in Figure 1. The rf power driving the transducer of the Bragg cell is modulated by a digitally controlled network of attenuators. The real and imaginary parts of each component of the input vector are stored in a buffer on the digital control board. On this digital control board the data are modified to correct for the acoustic attenuation in the Bragg cell and for non-uniformities in the transverse, horizontal intensity profile of the laser beam. The data are then clocked out to the attenuator network at 25.6 MHz. Immediately following the downloading of the last vector component, the information for the entire vector is represented by the longitudinal distribution of acoustic power in the Bragg cell. The laser is fired, and the vector becomes represented by the transverse, horizontal intensity distribution of the diffracted radiation. This diffracted radiation, following collimation, is incident on a rectangular array of apertures. The area of each aperture represents the real or imaginary part of a matrix element. The radiation transmitted through the aperture array mask is directed onto a linear detector array such that the radiation from each row of apertures falls on a single pixel of the detector array. The output vector is read out of the detector array, digitized, and uploaded to the host computer. In the host computer the data may be processed to correct for noise associated with: pixel-to pixel-variations in detector sensitivity, detector dark current, and for non-

Manuscript approved August 24, 1988.

uniformities in the vertical intensity distribution of the radiation field.

III. PERFORMANCE ANALYSIS

A. Laser Performance

The laser is a Multiheterostructure GaAlAs laser diode operating at 890 nm with a minimum rated peak radiant power of 12 Watts (at 300 K). The exit pupil of the laser diode is 400 μm by 2 μm. The laser is mounted so that its longitudinal axis is horizontal and the long axis of the exit pupil is vertical. This assures that the laser beam propagates horizontally with the greatest beam divergence in the horizontal plane. The system requires a laser that meets the following performance criteria:

energy per pulse	-sufficient to saturate the photodiode array after passing through the system.
duration of pulse	-sufficiently short to freeze the motion of the acoustic field in the Bragg cell during a laser firing.
repeatability	-there are no provisions to correct for pulse to pulse fluctuations in the beam profile. Thus, both the horizontal and vertical beam intensity profile must be highly repeatable.
firing rate	-fast enough to permit the laser to fire every 10 μs, the time needed to load a vector into the Bragg cell.

The relative horizontal intensity profile of the laser was measured using a 1024-element photodiode array (Reticon RL1024S). A typical horizontal intensity profile is shown in Fig. 2. The VMM uses the portion of this profile that extends approximately 112 pixels to either side of the beam axis. At the edges of this region the intensity dropped to 88 percent of the peak (center) value. At any pixel of the array, the pulse-to-pulse variation of the intensity was measured and found to be approximately 1%.

The full width at half maximum (FWHM) of the laser pulse (Fig. 3) is 10 ns, less than half of the 39 ns (164 μm) feature size in the Bragg cell (see Section III. B.). Since one-to-one imaging of the Bragg cell onto the aperture array mask was used, the horizontal, center-to-center aperture spacings were made equal to the feature size (164 μm) in the Bragg cell (Fig. 4). During the 20 ns (see Fig. 3) duration of the laser pulse the features of the acoustic field in the Bragg cell, and thus the features of the diffracted radiation, travel about 82 μm, half the center-to-center aperture spacing. To prevent effects of

this motion from reaching the detector, the maximum width of an aperture is limited to 82 μm.

A discussion of the power requirements placed on the laser in connection with the detector array performance can be found in Section III. D.

B. Bragg Cell, RF Attenuator Network, and Digital RF Controller

The information is encoded in the radiation field via an Interaction Model AOD150 dense flint glass Bragg Cell. The cell's specifications are listed in the table below.

BRAGG CELL SPECIFICATIONS

entrance pupil	45 mm x 3 mm
center frequency	150 MHz
acoustic speed	4100 m/s
measured attenuation (at 150 MHz)	≈2.3 dB/cm
bandwidth	100 MHz
time bandwidth product	1000

The power level of the 150 MHz rf signal that drives the transducer is determined by the state of the digitally controlled rf attenuator network (see Fig. 5). Since the output of the digital controller is clocked at 25.6 MHz, in 10 μs the rf power level is specified 256 times (at 39 ns intervals). Since the speed of sound in dense flint glass is 4100 m/s, the acoustic field generated in a 10 μs interval is distributed over a 4.1 cm length of the cell. The digital controller thus partitions the acoustic field into 256 sections (features), each section being 164 μm long. The instantaneous acoustic power in any particular feature is the product of the acoustic power output of the transducer when that feature was clocked, and the attenuation of the signal after propagating from the transducer to its present position of the feature. The intensity of the optical radiation diffracted by the acoustic field varies with acoustic power. Thus the horizontal intensity profile of the diffracted optical field is also partitioned into 256 sections.

The 150 MHz rf signal driving the Bragg cell transducer is gated through the attenuator network (see Fig. 5) by eight digitally controlled switches. The status (on/off) of each switch is determined by a digital control line. The controller receives data and control information from an IBM PC-AT via a National Instruments GPIB interface. The data consist of two vectors (arrays), VectorData and CorrectionData. These arrays are stored in high speed memory buffers which reside on the digital control board. VectorData is the VMM input vector. In

order to correct for both the acoustic attenuation within the Bragg cell and nonuniformities in the horizontal intensity profile of the incident radiation, the elements of VectorData are multiplied by the corresponding elements of CorrectionData. For this purpose the controller has a resident, high speed 8 x 8 bit multiplier (MC10901). Each byte of the output of the digital control board is the high order byte of the product of corresponding elements of VectorData and CorrectionData. Each bit of these output bytes determines the state of the corresponding rf switch in the attenuator network.

The diffraction efficiency of the Bragg cell varies as the square of the sine of the square root of the acoustic power[1]. For this particular Bragg cell driven at 159 MHz this relation is

$$\frac{I_d}{I_o} = \sin^2\sqrt{(0.736P)} ,$$

where I_d is the diffracted intensity, I_o is the incident intensity, and P is the acoustic power in watts. The prototype VMM is restricted to operate in the domain where the diffraction efficiency varies linearly with acoustic intensity. If eight bit accuracy is to be maintained, this restriction limits the acoustic power to 16 mW and the diffraction efficiency to 1.2%. Higher diffraction efficiencies might be achieved by driving the Bragg cell at higher power levels while correcting for the nonlinearities. These corrections would involve preprocessing the signal using a high speed look up table. In the VMM prototype this enhancement was not implemented.

The attenuation network consists of eight rf attenuators arranged in parallel branches (Fig. 6). The attenuation in branch i+1 is 6 dB greater than that in branch i, i = 1,..,7. Consequently, the output voltage of branch i+1 is half that of branch i. When the voltages are recombined (in phase), the voltage of the combined signal is the sum of the voltages of the branch signals. Thus the voltage of the network output signal is $K \cdot V_1$, where the integer K = 0,...,255, and V_1 is the output voltage of the branch with the greatest attenuation. And thus the power level of the network output signal is $K^2 P_1$ where P_1 is the power output of the branch with output voltage V_1.

As indicated above, it is the voltages (amplitudes) that add when the branch signals combine. Since power is proportional to the square of the voltage, equal increments of voltage imply unequal increments in power. Ideally, it is the increments in rf power that should be equal. However, it does not appear feasible to configure eight branches of attenuators to produce 256 equally spaced power levels.

In the Bragg cell, the acoustic power is attenuated at 2.3 dB per cm. Thus the attenuation over the 4.1 cm active

length of the cell is 9.7 dB (90%). When the elements of the array VectorData have identical values, the horizontal intensity profile of the diffracted radiation field should be uniform. For a uniform input vector, the elements of CorrectionData must cause a monotonic increase in the attenuation of the network, with a maximum attenuation of 9.7 dB. To accomplish this the elements of CorrectionData must vary from 255 to 86 according to the relation

$$K[I] = 255 \cdot 10^{-0.05\beta VI/f} .$$

In this relation the attenuation coefficient β is 2.3 dB/cm, the sound velocity V is 4100 m/s, the clock counter I is the output of a MOD 256 counter, and the clock frequency f is 25.6 MHz. Since the K[I]'s are integers, the values obtained from the expression must be appropriately rounded. The value of K[255] is 86.

Consider the case when VectorData[I] = 255 (I = 0,...,255) and the elements of CorrectionData are optimally selected to produce an acoustic field, and thus a diffracted infrared beam, with a uniform intensity profile. The distribution of acoustic power at the time the laser is fired can be found in column tnree of Table I. This distribution has a mean of 7476 and a standard deviation of 41. Thus the 7476 units of available acoustic power can be divided into, at most, 91 (7476/82) distinct values, each value an integral multiple of 82 units. However, all 91 of these values cannot be realized because the attenuator network does not have sufficient resolution. The attenuator network outputs 7396 (86^2) units of pcwer when the datum written to it is 86 and 7225 (85^2) units when the datum is 85. Thus the minimum change in power that the attenuator network can deliver is 171 (7396-7225) units. This implies that the 7476 units of available acoustic power can be divided into no more than 43 (7476/171) values. Consequently, there is a corresponding resolution to the intensity level of the diffracted optical radiation.

Let I_1 denote the optical intensity diffracted by the segment of the Bragg cell nearest the transducer when the rf power driving the transducer is P_1. The diffracted optical intensity level I_d may range from zero to $86^2 I_1$ while the resolution of this intensity level is $171I_1$. To provide significantly distinct levels of diffracted intensity, the rf power must be incremented by integral multiples of $171P_1$. Thus the diffracted intensity level must lie between zero and $86^2 I_1$, and must be an integral multiple of $171I_1$. That is:
$I_d = N \cdot 171I_1 \pm 86I_1$, N=0,...,43.

With only 44 distinct levels of diffracted intensity, the elements of the VMM's output vector are limited to less than 6-bit accuracy. In order to achieve the specified 8-bit accuracy, a full 256 significantly distinct levels of diffracted intensity

must be available. Increases in the number of distinct levels of diffracted intensity can be achieved by: substituting a Bragg cell with less attenuation, controlling the rf power in a manner that results in rf power levels with equal increments, increasing the number of available rf power levels, and/or fabricating an infrared filter with a spatial variation in transmitted intensity appropriate to correct for the effects of acoustic attenuation within the Bragg cell.

The horizontal intensity profile of the radiation incident on the Bragg cell varies by about 12% over the 4.1 cm length of the cell. This variation is corrected for on the rf control board by appropriately modifying the elements of CorrectionData. The additional rf attenuations used to provide this correction are relatively small and will not require CorrectionData elements less than 86.

It should be noted that the attenuation board outputs 256 equal increments of voltage rather than power. In this regime, the power for the maximum output voltage is 2^{16} times larger than the smallest increment between power levels (which is equal to the smallest nonzero power level). Thus the attenuation board must be calibrated to an accuracy of one part in 2^{16}.

C. Aperture Array Mask

The product of two complex numbers X and A can be implemented via matrix-vector products involving only real numbers. Let

$$A = a^R + ia^I, \tag{1}$$

and

$$X = x^R + ix^I. \tag{2}$$

Then

$$P=A\cdot X= (a^Rx^R - a^Ix^I) + i(a^Rx^I + a^Ix^R) = p^R + ip^I, \tag{3}$$

or,

$$\begin{vmatrix} p^R \\ p^I \end{vmatrix} = \begin{vmatrix} a^R & -a^I \\ a^I & a^R \end{vmatrix} \begin{vmatrix} x^R \\ x^I \end{vmatrix} . \tag{4}$$

In the VMM, all complex multiplies are executed with this algorithm. Each complex element of the vector is represented as a two-element real vector and each complex matrix element is represented as a 2 x 2 real matrix. Thus a 128 complex-element vector is represented by a 256 real-element vector and a 128 x 128 complex-element matrix is represented as a 256 x 256 real-element matrix.

When a pulse of radiation of uniform intensity I is incident on an aperture of area S, the transmitted energy per pulse is proportional to the product I·S. In the VMM, the matrix is represented as a rectangular array of 256 x (256 + 1) apertures (see Fig. 7). The area of an aperture determines the value of the real number it represents. An offset is used to represent signed numbers: aperture areas less then a specified aperture size S_o represent negatively valued numbers while aperture areas greater than S_o represent positively valued numbers. The first row of apertures, each of area S_o, allows calibration for the bias or offset associated with the choice of S_o. In the postprocessing of the electronic output, all levels are compared to this bias level. The input vector is represented by the transverse, horizontal intensity distribution of the radiation field incident on the aperture array. This horizontal intensity distribution is divided into 256 segments (features), each segment incident upon a single column of apertures. The intensity level of a segment corresponds to the value of the number it represents. A specified intensity I_o corresponds with the value zero, while intensities less/more than I_o correspond to negatively/positively valued numbers.

A vector matrix product can be represented as follows:

$$y_i = \sum_j a_{ij}\, x_j \qquad (5)$$

where the quantities are 8-bit signed integers.

Let $a_{ij}' = a_{ij} + B_1$, $x_j' = x_j + B_2$, and

$$y_i' = \sum_j (a_{ij} + B_1)\,(x_j + B_2)\ . \qquad (6)$$

To insure that the values of the primed parameters defined above are non-negative, the values of the bias terms B_1 and B_2 are both set to 127. The values of these primed quantities are represented by aperture area and radiation intensity. Combining expressions (5) and (6) yields a relation expressing y_i in terms of y_i' and a sum involving three bias-dependent terms.

$$y_i = y_i' - \sum_j (a_{ij}\, B_2 + B_1\, x_j + B_1 B_2) \qquad (7)$$

In order to determine the values of the voltages associated with B_1 and B_2 we input the zero vector ($x_j = 0$ for all j) in the VMM. With a zero input vector the intensity of the radiation incident on each column of the aperture array is I_o (corresponding to B_2). The radiation from the bias row of apertures is collected at the zeroth pixel of the detector array. The detector output voltage V_1 associated with the charge integrated by this radiation during one laser pulse corresponds to the value of the term $y_0 = 0$. This voltage also corresponds to the value of the term $V_1 = y_0' = N \cdot B_1 B_2$, where N (=256) is the number of apertures in

the bias row. This zero vector, when applied to the bias calibration row at the mask (i=0) yields the term $V_1 = N \cdot B_1 B_2$, where N (=256) is the number of elements in a row. Since voltage levels corresponding with both B_1 and B_2 are needed, a second calibration measurement is required to specify voltage levels corresponding to both B_1 and B_2. This is done by multiplying the matrix by a vector whose elements are all equal to the maximum value possible. That is, $x_j = 128$ for all j. Then Eq. (7) yields $V_2 = y_0' = N \cdot B_1(128 + B_2)$. Simultaneously solving for the bias terms results in the relations

$$B_1 = \frac{V_2 - V_1}{128N} \qquad B_2 = \frac{128V_1}{V_2 - V_1} \ .$$

As each aperture represents an 8-bit signed number, there are 256 distinct aperture sizes allowed. The architecture is such that each aperture has a height of 50 μm and a width that may vary between zero and 82 μm (Fig. 7). The optical power passing through an aperture is proportional to the product of the width of the aperture and the intensity of the incident radiation. However, due to diffraction, not all the transmitted power is delivered to the detector. The aperture widths are selected so that when the transverse intensity distribution of the incident radiation is uniform and constant, the power distribution delivered to the detector via each aperture will be one of 256 values which are equally spaced.

A cylindrical and a spherical lens combination (Fig. 8) collects the radiation from the aperture array and directs it to the linear detector array. With this arrangement the detector array is positioned in the image plane of the aperture array mask vertically and the Fourier transform plane of the aperture array mask horizontally. Consider the optical power delivered to a detector pixel from a single aperture. Assuming the aperture to be uniformly illuminated, the horizontal intensity distribution (Fig. 9) at the detector pixel is proportional to the square of a sinc function

$$\text{Relative Intensity}(x) = \text{sinc}^2(x/x') \qquad (8)$$

where x' = (lower case lambda) f/w, lambda being the wavelength, f the focal length and w the aperture width. The incident relative power delivered to the pixel, the integral of the relative intensity over the full 2500 μm width of the detector pixel, varies with aperture width w. The aperture widths w_n (n=0,...,255) are selected to produce a relative power spectrum $P_n = nP_o/255$, where P_o is the relative power incident on the pixel when the aperture width w is the maximum 82 μm. This relation is

$$P_n = nP_o/255 = \int_{-1250\ \mu m}^{+1250\ \mu m} \text{sinc}^2(x/x_n')\, dx \ , \quad x_n' = f/w_n \ . \qquad (9)$$

The relative power constant P_0 is determined by integrating Eq. (9) when n is 255 and w_n is 82 μm. The values of the remaining w_n's (n=0,...,254) are determined numerically from Eq. (9).

An aperture array mask based on the above calculations and designed for calculating discrete Fourier transforms was fabricated using electron beam lithography. The output vector of the VMM, when used with this mask, is the discrete Fourier transform of the input vector.

D. Detector Array

The photodetector consists of a linear 1024 element photodiode array (Reticon RL1024S) with each photodiode measuring 25 μm by 2500 μm. The array is configured to be read out as 512 separate elements, each element consisting of an adjacent pair of pixels. The maximum readout rate of the array is 5 MHz. The widths and the center-to-center spacing of the pixels of the photodiode array influence the design of the aperture array mask as well as the supporting aperture-to-detector optics. In addition to the bias row, the aperture array mask contains 256 rows of apertures. The radiation from each row of apertures falls on a unique detector pixel pair. To prevent errors due to crosstalk, between each of these "active" pixel pair is a "dummy" pixel pair whose output is ignored. The radiant energy per pulse incident on an active pixel pair corresponds to an 8-bit integer, the real or imaginary part of an element of the output vector. The array-to-detector optics were designed to have a magnification of unity, thus the aperture array masks are designed so the center-to-center spacing of the rows is 100 μm, twice the center-to-center pixel pair spacing of the detector.

The saturation energy per unit area of the Reticon RL1024S is 50 nJ/cm^2. In order to utilize the detector's full dynamic range, the maximum integrated intensity per laser pulse should be sufficient to drive it to saturation. The equation describing this is:

$$P > \frac{\text{Saturation Energy}}{n_1 \, n_2 \, n_3 \, PW} ,$$

where PW is the pulse width of the laser and n_1, n_2, and n_3 are the optical efficiencies for the Bragg cell, the lenses and mirrors, and the aperture array mask. The maximum pulse width is 20 ns while n_1, n_2, and n_3 are estimated to be 0.012, 0.54, and 0.125. Thus, to drive the detector into saturation with a single laser pulse, a minimum laser power of one kilowatt is required. The supplied laser has a 10 ns pulse width and 12 watts of peak power (See Section III. A.), not all of which is incident upon

the entrance pupil of the Bragg cell. With the rf power driving the Bragg cell at a constant 3 W, we repeatedly fired the laser until the detector became saturated. Saturation was reached after approximately 100 shots. The diffraction efficiency at 3 W of rf power (≈1.5 W of acoustic power) is about 0.1. Unfortunately, a maximum rf power of ≈32 mW (16 mW of acoustic power) is necessary if the nonlinear terms in the relation between the diffraction efficiency and the acoustic power are not to detract from the specified eight bit accuracy. Using the 12 W laser with a pulse width of 10 ns, saturation should occur after some 550 laser firings. To saturate the detector with one laser firing at a pulse width of 10 ns would require a 6.6 KW laser. See the discussion at the end of Section III. B. that proposes a modification to reduce the required laser power.

It takes 10 μs to load a vector (256 bytes) into the Bragg cell (and 20 ns for the laser to fire). Since this process can be repeated continuously, a continuous serial transfer rate of 25.6 MHz seems feasible. However, because the maximum readout rate of the detector is 5 MHz, the maximum continuous throughput of the prototype is reduced from 10^5 vector matrix products each second to 10^4 products each second.

E. Imaging and Focusing Optics

The optics that image the mask onto the detector array (Fig. 8) consist of a cylindrical lens and a spherical lens, each with a 75 mm diameter and a 200 mm focal length. The cylindrical lens is positioned, with its axis horizontal, one focal length from the mask; the spherical lens is positioned two focal lengths from the mask; and the detector array is located one focal length from the spherical lens. With this configuration the plane of the detector coincides with the image plane of the mask (vertically) and with the Fourier transform plane (horizontally). Thus the radiation from each row of the mask falls onto a single pixel pair of the detector array.

To perform acceptably, the image of each mask row must fall on the corresponding pixel pair of the detector. Since the detector array contains 512 pixel pairs, the two lens combination must have a linear magnification of unity to one part in 512 (or 0.2%). This implies that the focal lengths of the two lenses be equal to within 0.2%. In assembling the prototype no attempt was made to accurately match the focal lengths. The image of the aperture array mask and the pixels of the detector array were found to be significantly out of registry (Fig. 10). Since the lenses are ≈ f/2.7, it is likely that additional difficulties with registry can be attributed to spherical aberration.

F. Data Acquisition and Post Processing

In the prototype the detector array is mounted on an EG&G Reticon (Model RC1024L) evaluation circuit board. The array

output was digitized via a 12-bit A/D converter and stored in a buffer resident in the host microcomputer. No attempt was made to process the data to correct for nonuniformities in the vertical distribution of the radiation or for pixel-to-pixel variations in detector sensitivity. To correct noise associated with the response of the detector to dark current, the output voltage associated with dark current was measured and subtracted from the data.

IV. SUMMARY

In most of our measurements the sequence of actions implemented was:

- The input vector and the correction vector were downloaded from the microcomputer to buffers on the rf control board.
- The detector array was initialized (scanned).[1]
- The corresponding elements of the input vector and the correction vector were multiplied and the products (sequentially) clocked into the Bragg cell via the rf attenuator network and transducer.
- The laser was fired.
- The detector array was read (scanned), and the output data were digitized and stored.

The prototype VMM's performance fell short of meeting its specifications. The causes of the shortcomings include:

- The acoustic attenuation (2.3 dB/cm) in the dense flint glass Bragg cell is unacceptably high.
- The increments in rf power levels are not equal. This reduces the dynamic range by at least a factor of two.
- Remaining within the linear region of the diffraction efficiency/acoustic power curve places an unacceptably low (1.2%) upper bound on the diffraction efficiency.
- The laser energy per pulse is two orders of magnitude too low to provide sufficient dynamic range at the detector.
- Due to poor optical design and component quality, the radiation field features were out of registration with the aperture and detector arrays.
- The detector readout rate (>100μs/vector) and digitization rate are unacceptably low, and there are no corrections for noise associated with: dark current, nonuniformities in the vertical distribution of the radiation, and variations in sensitivity from pixel-to-pixel.

Suggested remedies for some of these shortcomings are:

- Replace the dense flint Bragg cell with one made of TeO_2. The substitution of a longitudinal TeO_2 Bragg cell for the dense flint glass cell would decrease the acoustic

---

[1]. The array was initialized prior to firing the laser in order to minimize noise associated with both dark current and ambient radiation.

attenuation by 8 dB while increasing the diffraction efficiency per watt of acoustic power by a factor of 3.8. The acoustic velocity in longitudinal TeO_2 is 4200 m/s, almost the same as the 4100 m/s acoustic velocity in dense flint glass.

- Generate the 150 MHz signal that drives the Bragg Cell with a 300+ MHz 12-bit digital to analog (D/A) converter. To implement such an rf source, a high speed processor is needed to process the input vector data and thus correct for the nonlinearities in the diffraction efficiency/acoustic power relation. A D/A converter meeting the above specifications is beyond the reach of current technology.
- Select lenses with more closely matched focal lengths and less spherical aberration. Adequate corrections for spherical aberration will likely require higher f numbers (and longer focal lengths).
- Fabricate a detector array with a faster readout rate. Use real time hardware rather than post processing software to correct for noise associated with: dark current, nonuniformities in the vertical distribution of the radiation, and pixel-to-pixel variations in sensitivity.
- Obtain a laser source with more power and less pulse-to-pulse variation in power and/or beam profile. If laser diode arrays continue to improve they may prove to be suitable.

REFERENCES

1. Yariv, A., Quantum Electronics, 2nd ed. (Wiley, New York, 1975)

TABLE I

CORRECTION FOR THE ATTENUATION OF ACOUSTIC POWER

CLOCK COUNT	INJECTED POWER*	ATTENUATED POWER*	DEVIATION
I	$K^2[I]$	P_A**	$(P_A^2-\langle P_A^2\rangle)$
0	65025	7478	2
1	64516	7482	6
2	64009	7487	11
3	63504	7491	15
4	63001	7495	19
5	62500	7499	23
6	62001	7502	26
7	61504	7505	29
8	60516	7448	-28
9	60025	7450	-26
10	59536	7452	-24
.	.	.	.
.	.	.	.
.	.	.	.
247	7921	7401	-75
248	7921	7464	-12
249	7921	7528	52
250	7744	7422	-54
251	7744	7486	10
252	7744	7549	73
253	7569	7442	-34
254	7569	7505	29
255	7396	7396	-80
	MEAN	7476	
	STANDARD DEVIATION	41	

* Numbers represent relative values.

** $P_A = K^2[I] \cdot 10^{-0.1\beta V/f}$

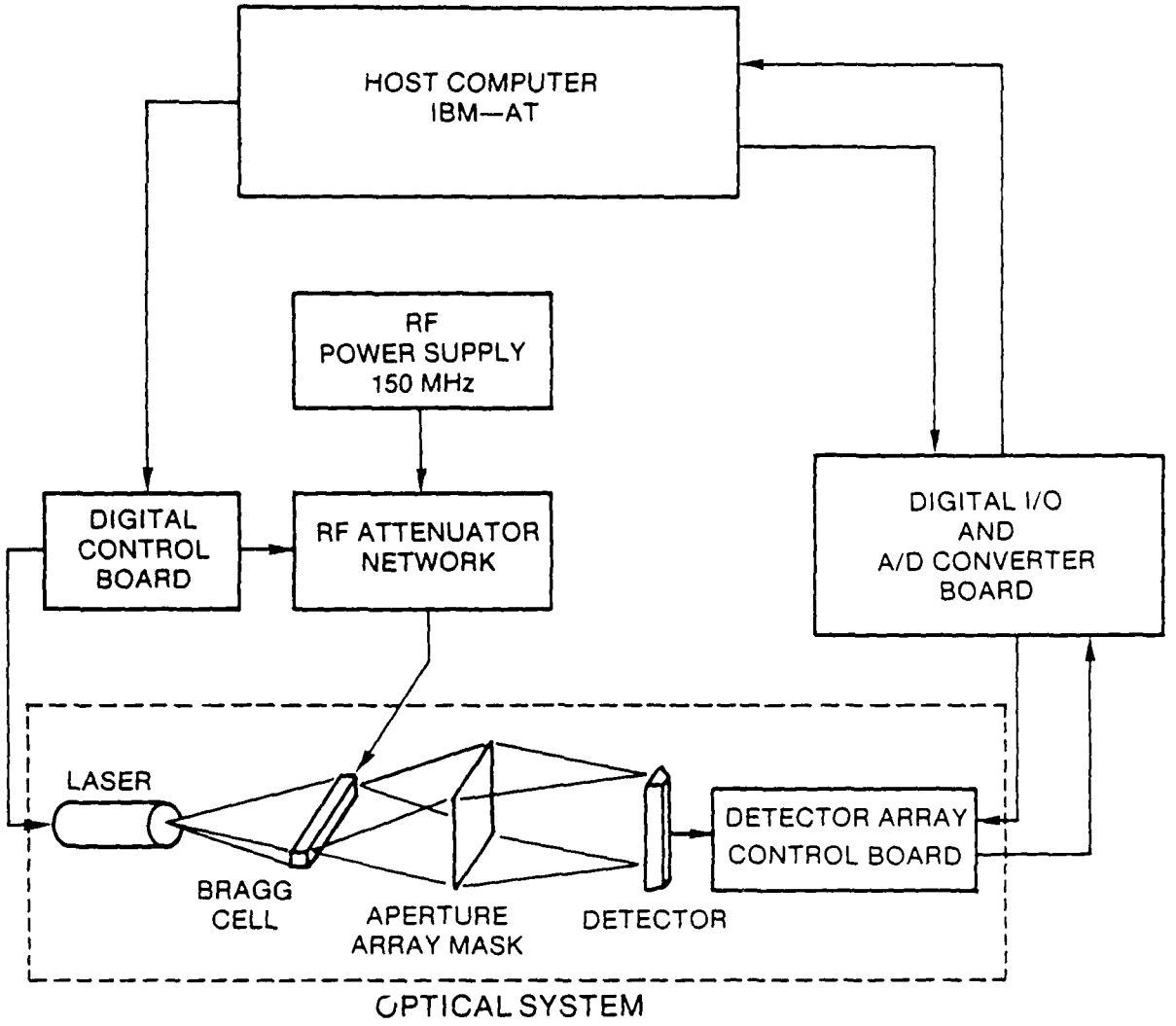

Fig. 1 — Schematic of system including the host computer, laser, Bragg cell, aperture array mask, detector, rf power supply, rf attenuator network, digital control board, and the digital I/O & A/D converter board.

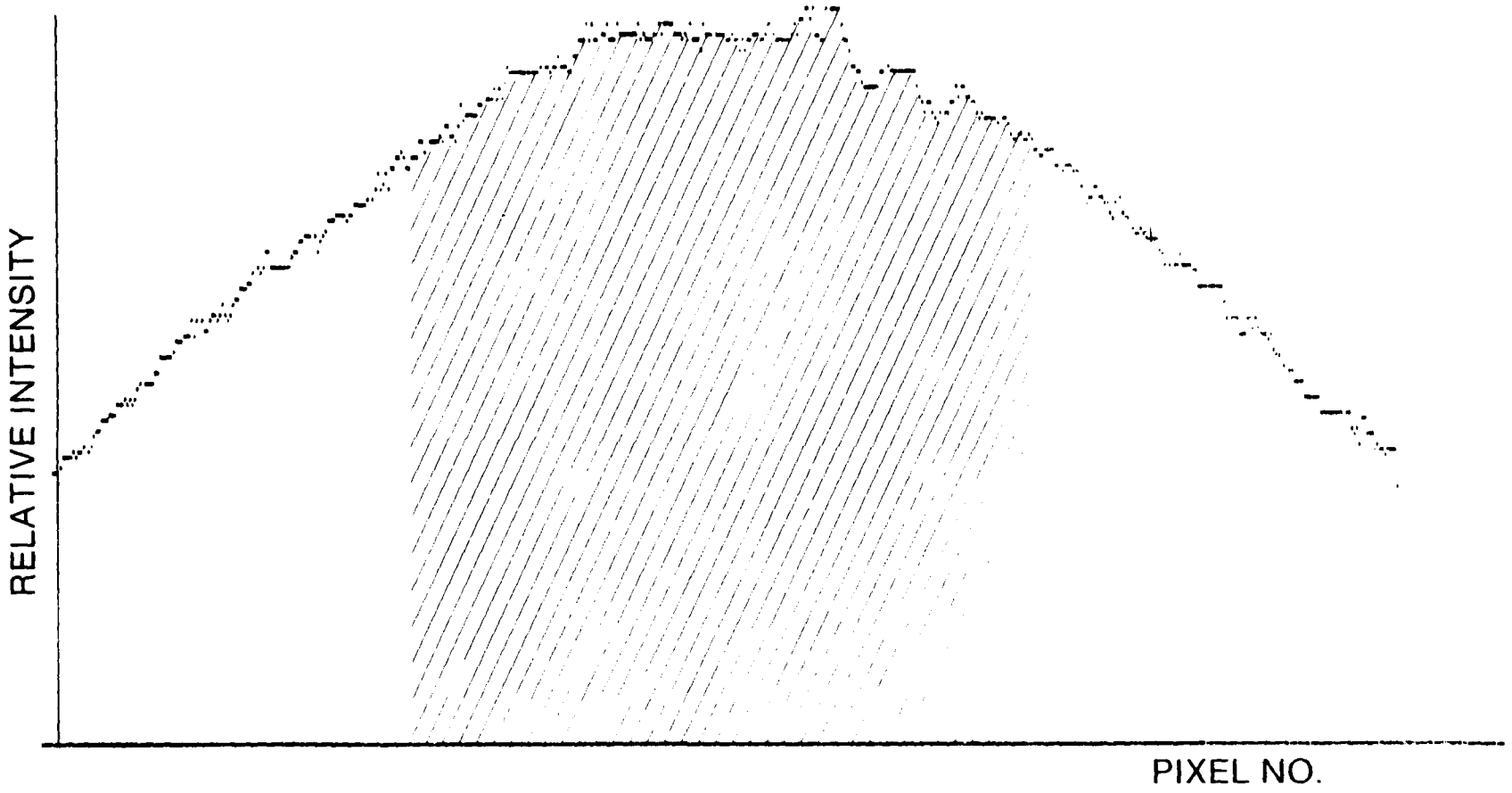

Fig. 2 — The horizontal intensity profile of laser beam measured a distance of 45 cm in front of the laser. Only the shaded region falls within the entrance pupil of the VMM's optical system.

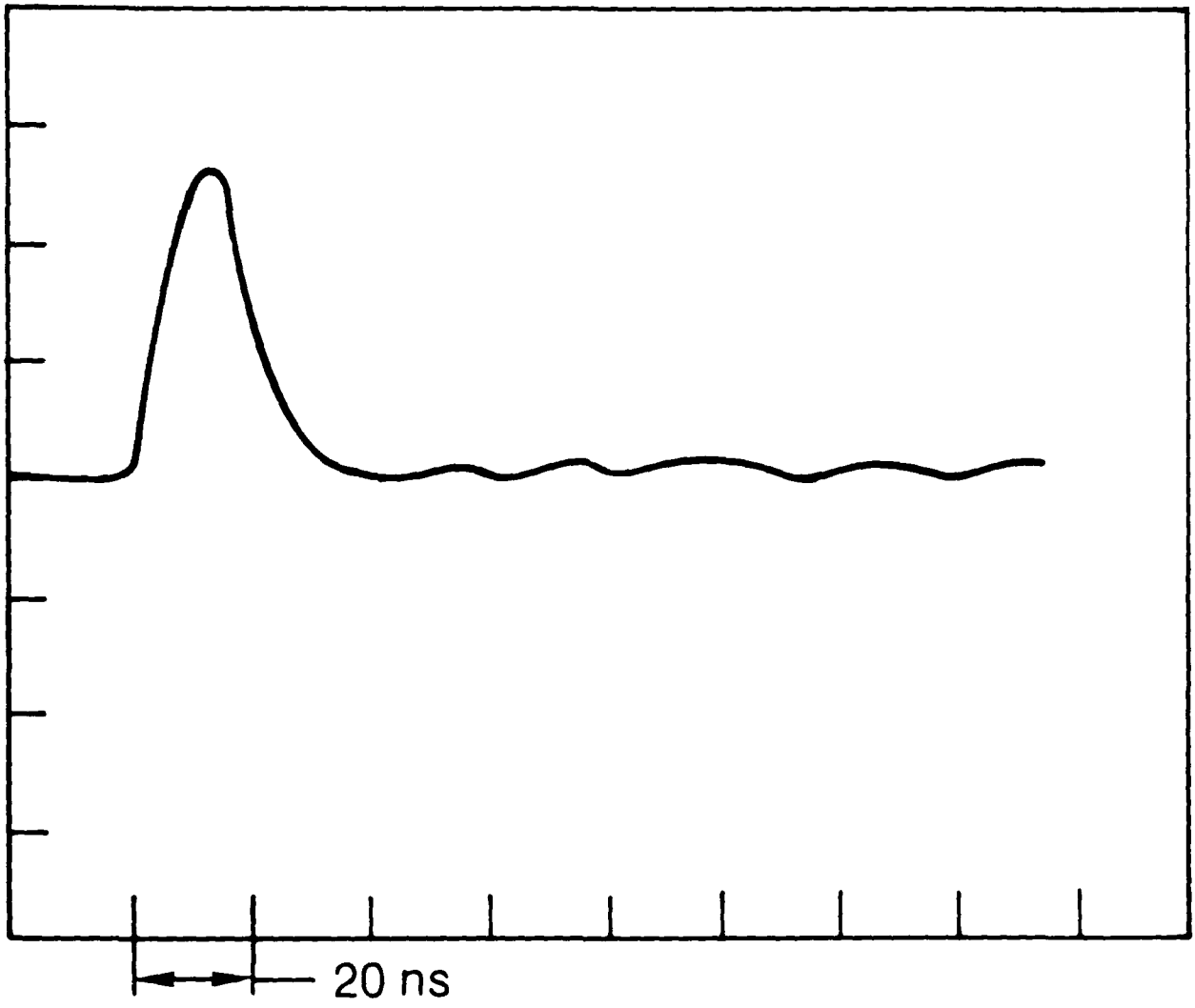

Fig. 3 — The intensity of the laser pulse versus time. The FWHM of the pulse is ≈ 10 ns.

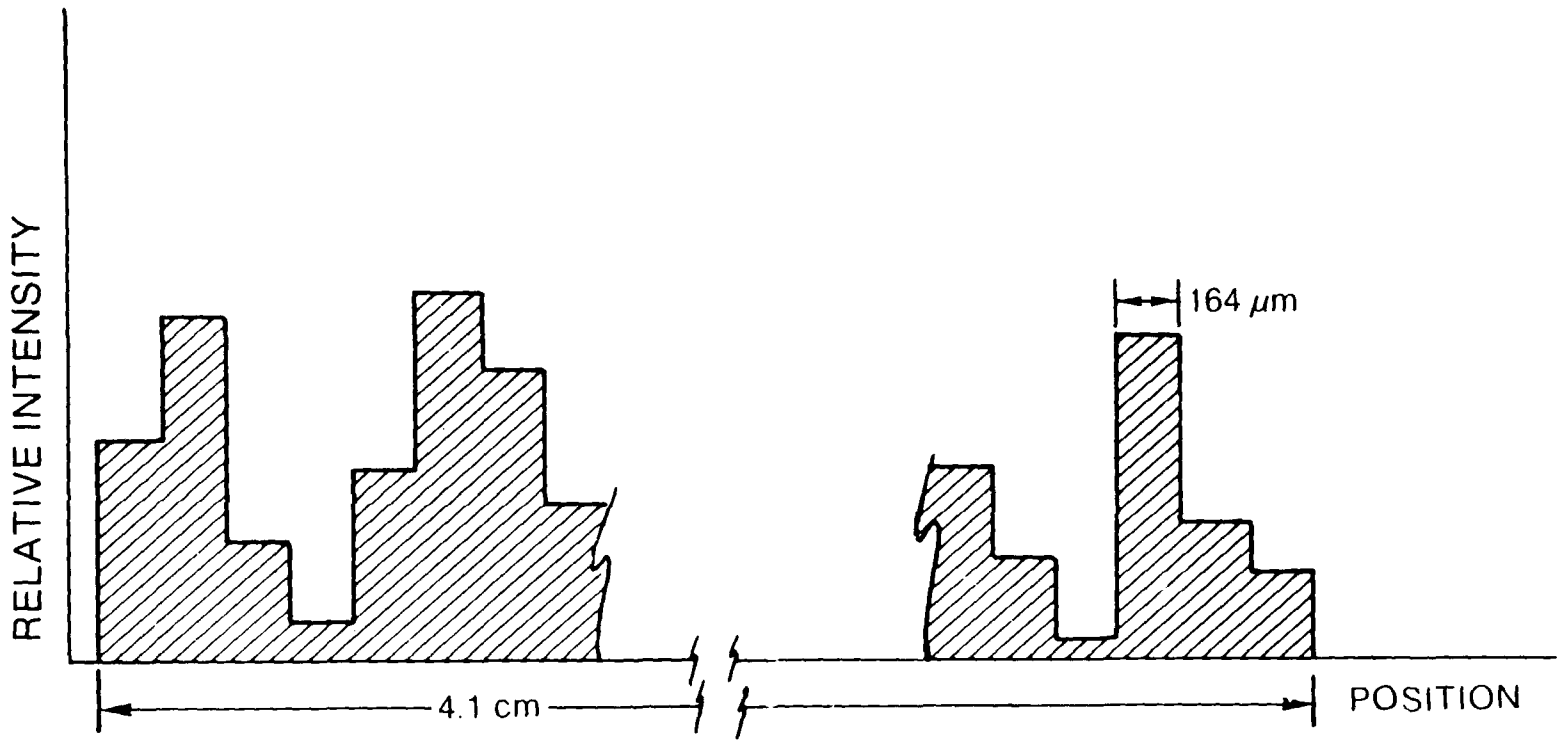

Fig. 4 — The feature of the acoustic signal in the Bragg cell are clocked in at a rate of 25.6 MHz (one every 39 ns). The features of the acoutic intensity distribution are 164 μm long.

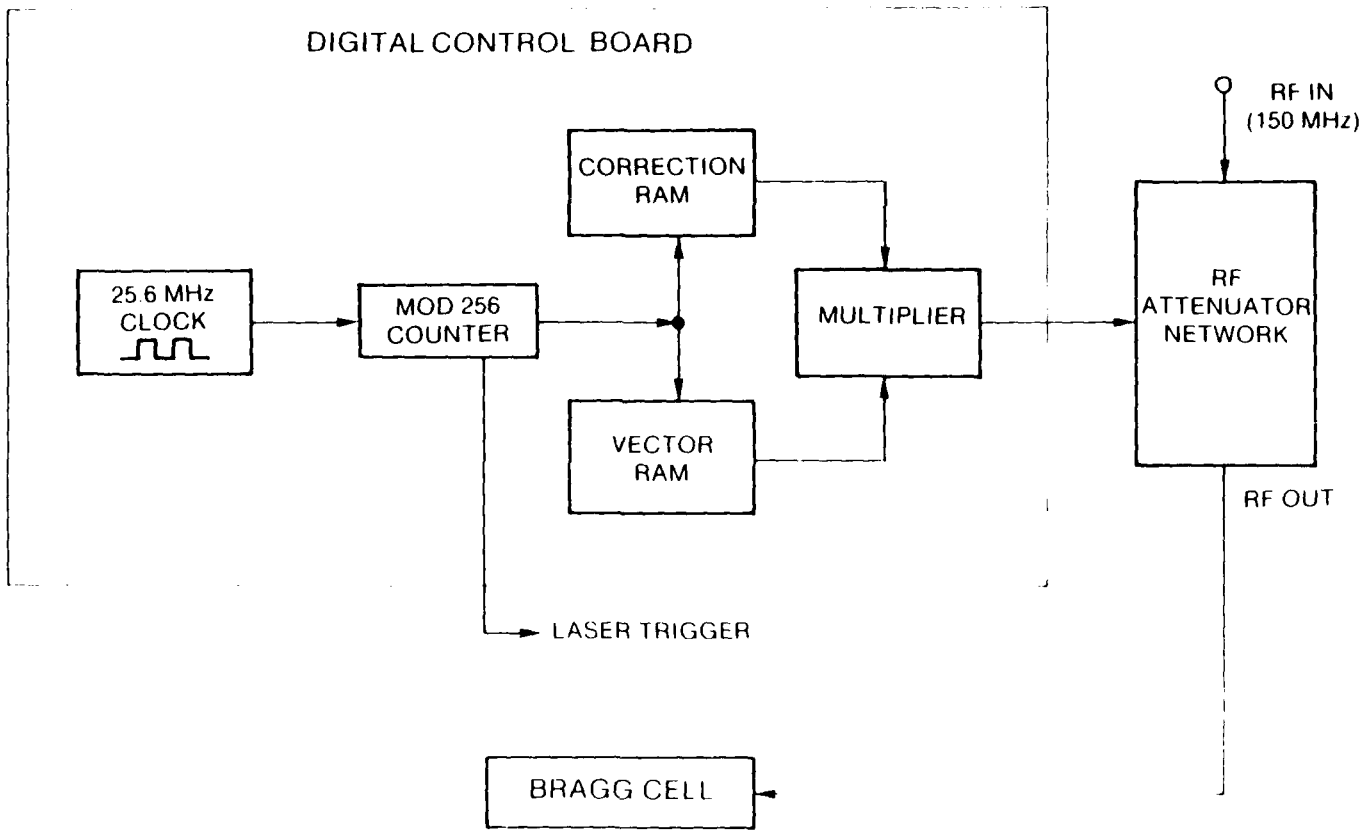

Fig. 5 — Schematic of the Bragg cell, the rf attenuator network, and the digital control board.

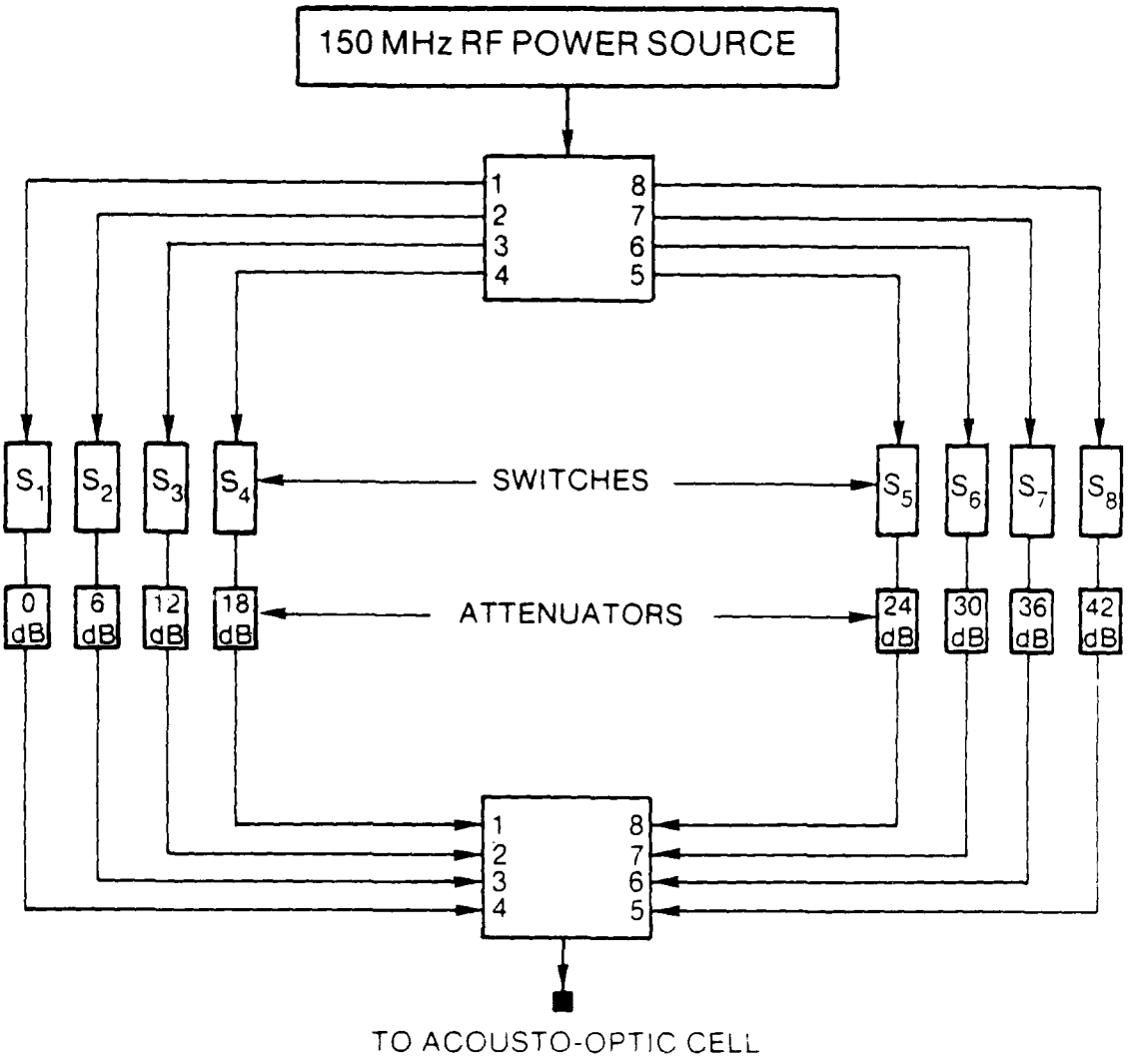

Fig. 6 — The rf attenuator network consists of eight branches, each successive branch having 6 dB additional attenuation. Each branch also contains a two state (on/off) digitally controlled switch and an adjustable phase shifter (not shown).

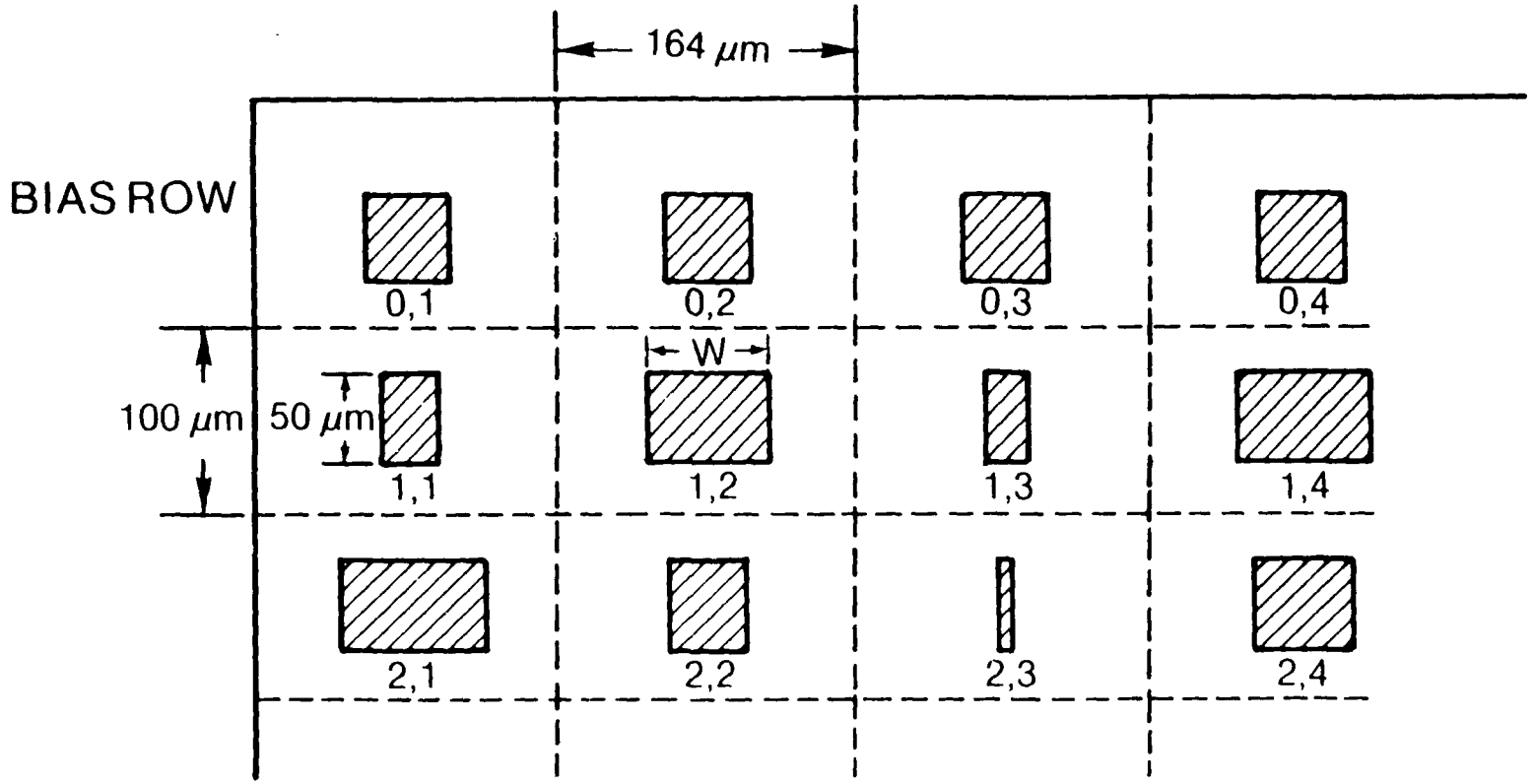

Fig. 7 — The aperture array mask consists of a rectangular array of 256 × (256 + 1) apertures each 50 μm high with widths up to 82 μm. The center-to-center spacings are 100 μm vertically and 164 μm horizontally.

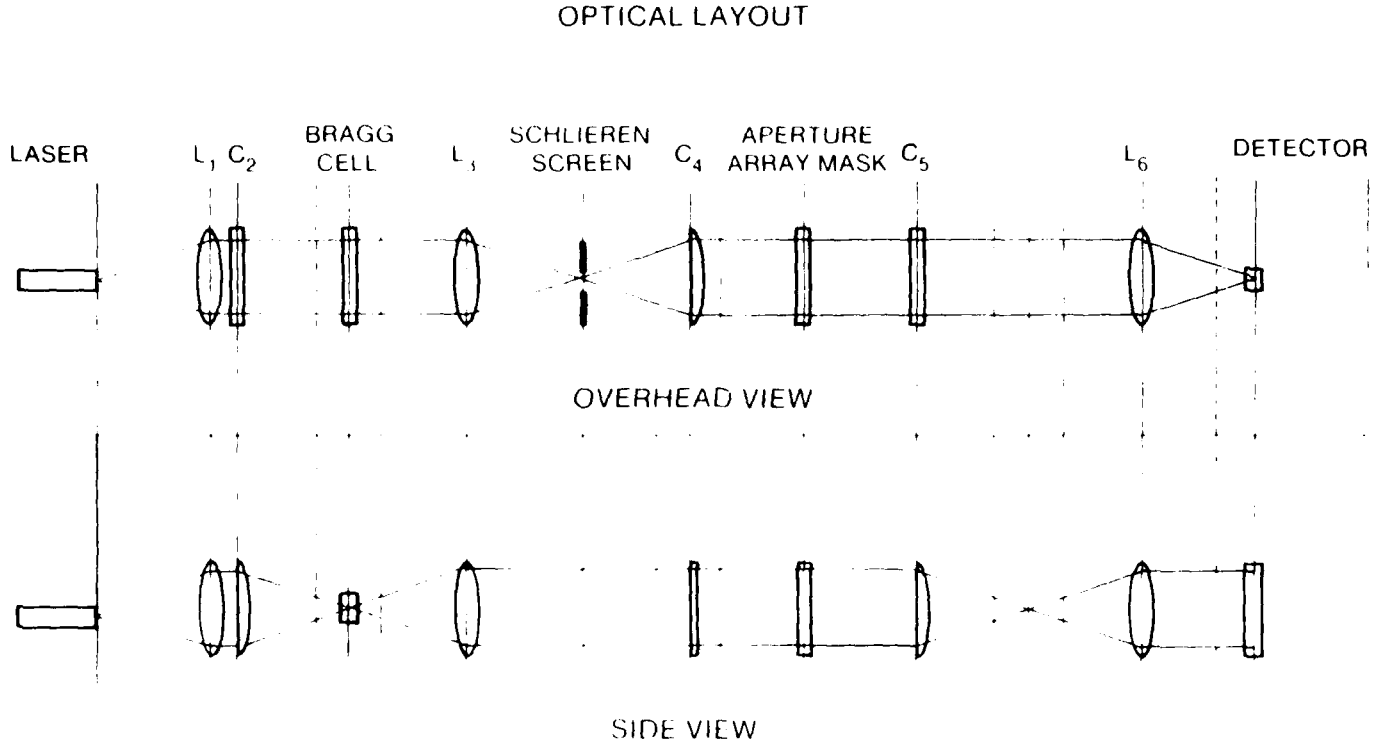

Fig. 8 — Overview of the optical layout. The spherical lenses are denoted with L's and the cylindrical lenses with C's. The lenses all have focal lengths of 200 mm which is the distance between the vertical lines on the grid to the right of C_1. There are front surface mirrors at the dotted lines, each deflecting the beam by 90°.

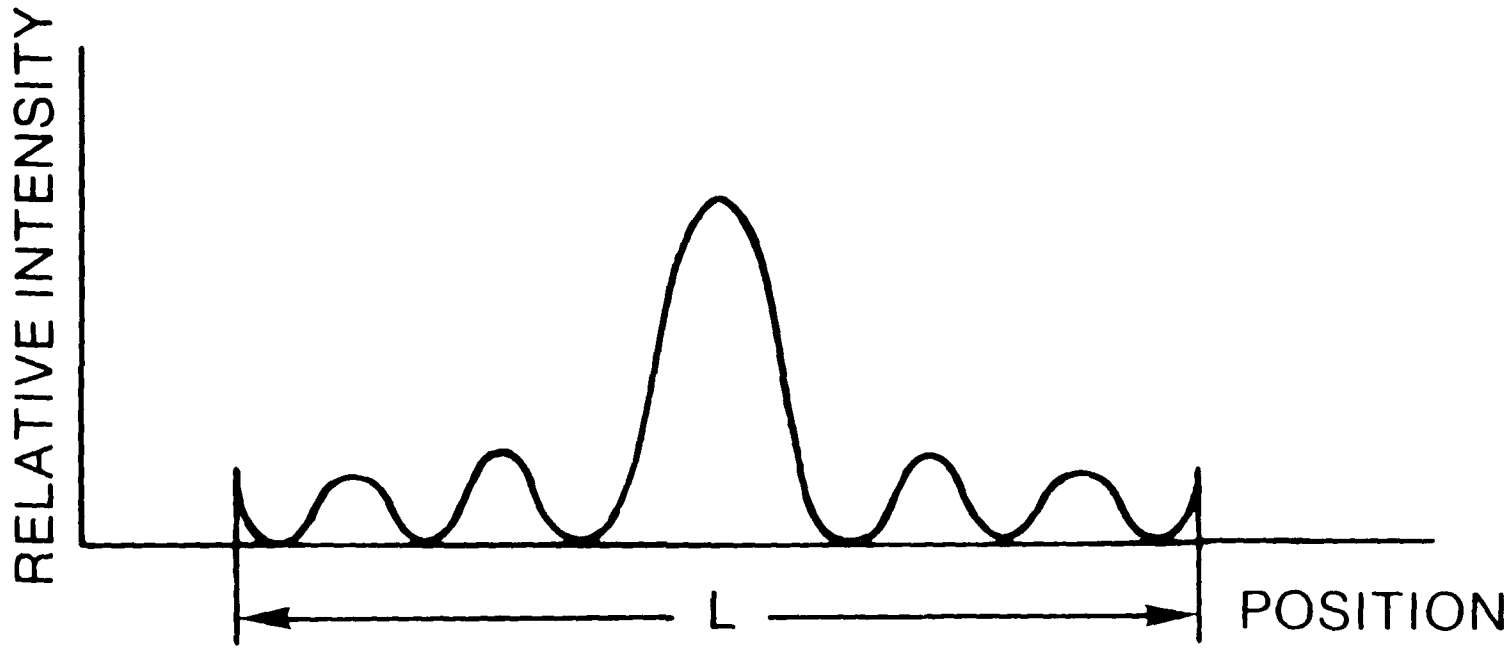

Fig. 9 — The intensity profile of the radiation from a single aperture is incident on a detector pixel pair. The length of a pixel pair, denoted L, is 2500 μm.

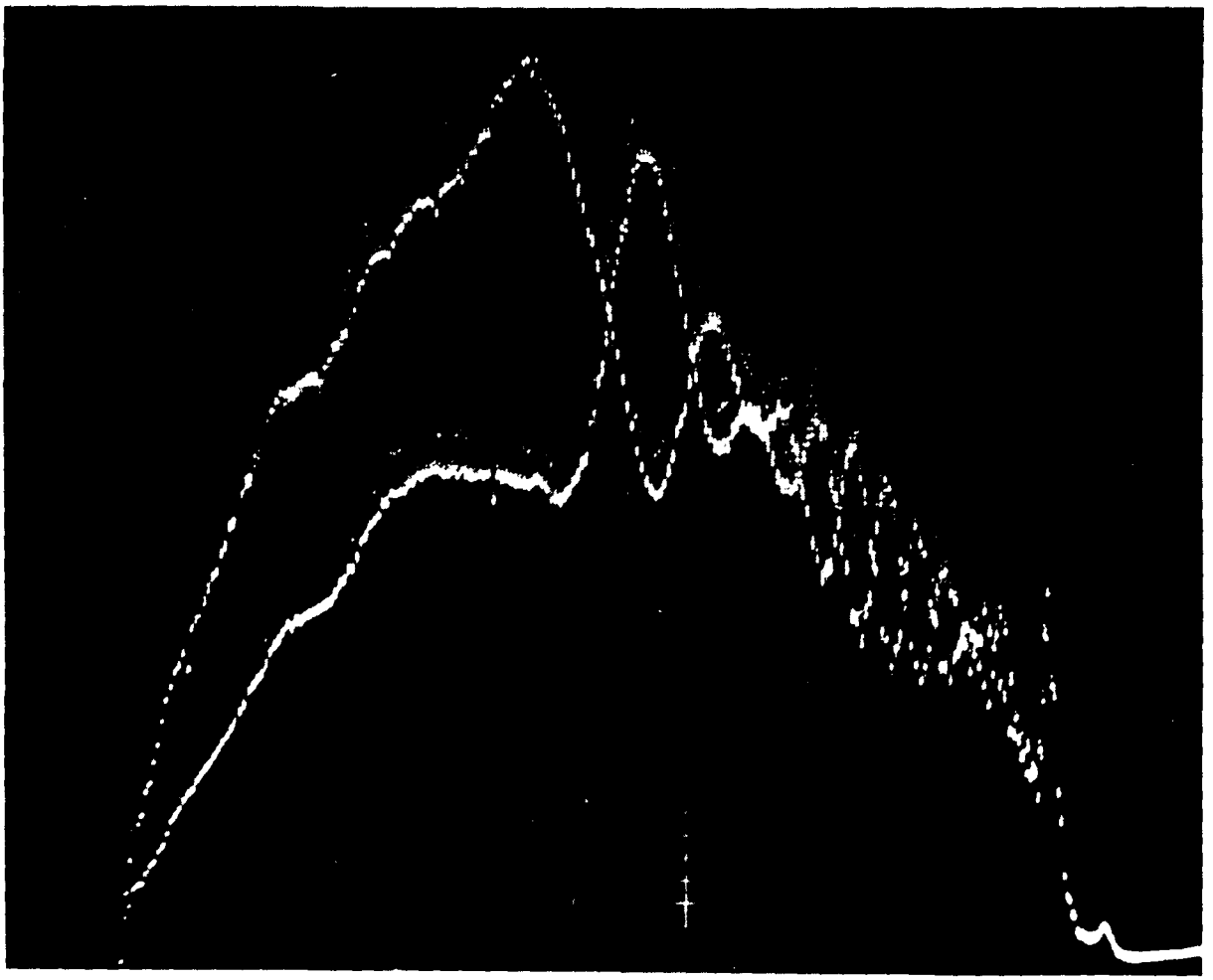

Fig. 10 — The readout of the array, displayed on an oscilloscope screen, shows that the registration of aperture row images and every other detector pair was inadequate. If the registry was adequate, the two curves would never cross.